

Article

Development of Biocompatible Ga₂(HPO₄)₃ Nanoparticles as an Antimicrobial Agent with Improved Ga Resistance Development Profile against *Pseudomonas aeruginosa*

Huda Alamri ^{1,2,*}, Guanyu Chen ¹ and Songping D. Huang ^{1,*}¹ Department of Chemistry and Biochemistry, Kent State University, Kent, OH 44240, USA; gchen10@kent.edu² Department of Chemistry, College of Science, University of Jeddah, Jeddah 21589, Saudi Arabia

* Correspondence: halamri@uj.edu.sa (H.A.); shuang1@kent.edu (S.D.H.)

Abstract: Ga(III) can mimic Fe(III) in the biological system due to its similarities in charge and ionic radius to those of Fe(III) and can exhibit antimicrobial activity by disrupting the acquisition and metabolism of Fe in bacterial cells. For example, Ga(NO₃)₃ has been proven to be effective in treating chronic lung infections by *Pseudomonas aeruginosa* (*P. aeruginosa*) in cystic fibrosis patients in a recent phase II clinical trial. However, Ga(NO₃)₃ is an ionic compound that can hydrolyze to form insoluble hydroxides at physiological pH, which not only reduces its bioavailability but also causes potential renal toxicity when it is used as a systemic drug. Although complexation with suitable chelating agents has offered a varying degree of success in alleviating the hydrolysis of Ga(III), the use of nanotechnology to deliver this metallic ion should constitute an ultimate solution to all the above-mentioned problems. Thus far, the development of Ga-based nanomaterials as metalloantibiotics is an underexploited area of research. We have developed two different synthetic routes for the preparation of biocompatible Ga₂(HPO₄)₃ NPs and shown that both the PVP- or PEG-coated Ga₂(HPO₄)₃ NPs exhibit potent antimicrobial activity against *P. aeruginosa*. More importantly, such polymer-coated NPs do not show any sign of Ga-resistant phenotype development after 30 passes, in sharp contrast to Ga(NO₃)₃, which can rapidly develop Ga-resistant phenotypes of *P. aeruginosa*, indicating the potential of using Ga₂(HPO₄)₃ NPs a new antimicrobial agent in place of Ga(NO₃)₃.

Keywords: Ga-based antimicrobial nanoparticles; antimicrobial resistance (AMR); top-down synthesis of nanomaterials; Ga-resistant bacterial phenotypes



Citation: Alamri, H.; Chen, G.; Huang, S.D. Development of Biocompatible Ga₂(HPO₄)₃ Nanoparticles as an Antimicrobial Agent with Improved Ga Resistance Development Profile against *Pseudomonas aeruginosa*. *Antibiotics* **2023**, *12*, 1578. <https://doi.org/10.3390/antibiotics12111578>

Academic Editors: Viviana Cafiso and Floriana Campanile

Received: 30 June 2023

Revised: 17 September 2023

Accepted: 21 September 2023

Published: 30 October 2023



Copyright: © 2023 by the authors. Licensee MDPI, Basel, Switzerland. This article is an open access article distributed under the terms and conditions of the Creative Commons Attribution (CC BY) license (<https://creativecommons.org/licenses/by/4.0/>).

1. Introduction

Antibacterial resistance has dramatically increased in the past several decades. This situation has led to an increased rate of morbidity and mortality caused by bacterial infections. Bacteria can rapidly evolve to develop new tactics to resist antibiotics and survive, which lowers the efficiency of existing antibiotics [1,2]. A recent report showed that more than one-third of clinical isolates of the Gram-negative bacterium *Pseudomonas aeruginosa* (*P. aeruginosa*) are now resistant to three or more antibiotic drugs [3]. The situation is very similar for other pathogenic organisms such as the Gram-positive *Staphylococcus aureus* (*S. aureus*), which is the cause of ~10% of hospital-acquired infections [4]. The number of infections caused by multidrug-resistant *S. aureus* (MRSA) has increased, with an increasing number of annual deaths related to MRSA infections [1]. Such problems are greatly worsened by the fact that the number of antibiotics approved for clinical use and in the drug development pipeline has dramatically declined over the past three decades [5]. There is an urgent need to develop new-generation antimicrobial agents with novel antimicrobial targets in order to win the battle against the rising antimicrobial resistance (AMR). Metalloantibiotics may offer a unique opportunity to hit the antimicrobial targets that are untouched by conventional antibiotics [6,7]. For example, targeting the acquisition and metabolism of iron by gallium has now been proven to be a viable approach

to developing new metalloantibiotics to overcome AMR [8–11]. Due to the similarities of Ga(III) and Fe(III), including their identical ionic charge and comparable ionic radii ($\text{Ga}^{3+} = 0.62 \text{ \AA}$ vs. $\text{Fe}^{3+} = 0.65 \text{ \AA}$ for the high-spin electron configuration), Ga(III) can act as an Fe(III) mimic. However, Ga(III) cannot be reduced to Ga(II) under the physiological conditions to perform the redox reactions required of many enzymes and proteins that contain Fe as a cofactor. Consequently, the binding of Ga to Fe-containing enzymes and proteins will disrupt iron metabolism, thus affecting certain biological processes that are critical for bacterial survival and growth [12–14]. Recently, $\text{Ga}(\text{NO}_3)_3$, a clinical drug initially approved by the FDA for the treatment of hypocalcemia in cancer patients, has successfully completed a phase II clinical trial for the treatment of chronic lung infections by *P. aeruginosa* in cystic fibrosis patients [11]. However, as an ionic salt, there are several disadvantages of using $\text{Ga}(\text{NO}_3)_3$ as a systemic drug, including (i) the lack of hydrolytic stability at physiological pH as the Ga^{3+} ion can readily hydrolyze to form insoluble hydroxides to reduce its bioavailability; (ii) a relatively short half-life in the blood stream due to the high glomerular filtration rate of this small cation; and (iii) potential nephrotoxicity and cause of visual and hearing loss due to hydrolysis [15,16]. Although complexation with suitable chelating agents (e.g., maltol) has offered a varying degree of success in alleviating the hydrolysis of Ga(III) [17–19], the use of nanotechnology to deliver this metallic ion should constitute an ultimate solution to all the above-mentioned problems [20–22].

In this publication, we report on our efforts to develop biocompatible Ga-based nanoparticles (NPs) containing hydrogen phosphate to overcome the shortcomings of $\text{Ga}(\text{NO}_3)_3$. The potassium salt of hydrogen phosphate (i.e., dipotassium phosphate, or K_2HPO_4) is widely used as an emulsifier, stabilizer, texturizer and chelating agent in the food industry. For example, K_2HPO_4 is found in many imitation dairy creamers, dry powder beverages, mineral supplements and milk products, to prevent calcium from precipitating out, etc. The two main objectives of this study are (i) to explore the possibility of developing $\text{Ga}_2(\text{HPO}_4)_3$ NPs as a broad-spectrum antimicrobial agent through their surface coating by a suitable polymer, as opposed to $\text{Ga}(\text{NO}_3)_3$, which has been known to be only active against Gram-negative bacteria such as PA; and (ii) to investigate whether $\text{Ga}_2(\text{HPO}_4)_3$ NPs would exhibit a delay in the development of Ga-resistant phenotypes of PA bacteria, as the rapid development of Ga-resistant phenotypes of PA bacteria treated with $\text{Ga}(\text{NO}_3)_3$ has become a genuine concern for its future clinical use. We show that the PVP- or PEG-coated $\text{Ga}_2(\text{HPO}_4)_3$ NPs exhibit potent antimicrobial activity against *P. aeruginosa* but are rather ineffective against SA. More importantly, such coated NPs do not show any sign of Ga-resistant phenotype development after 30 passes. In sharp contrast, Ga-resistant phenotypes of PA bacteria treated with $\text{Ga}(\text{NO}_3)_3$ emerge rather rapidly in PA bacteria that are treated with $\text{Ga}(\text{NO}_3)_3$, i.e., after five passages. Overall, $\text{Ga}_2(\text{HPO}_4)_3$ NPs still have desirable characteristics for use as a new antimicrobial agent against PA in place of $\text{Ga}(\text{NO}_3)_3$.

2. Results and Discussion

2.1. Determination of the Chemical Composition of the Reaction Product between $\text{Ga}(\text{NO}_3)_3$ and K_2HPO_4 Using the Conductimetric Titration

Based on the law of definite proportions, when $\text{Ga}(\text{NO}_3)_3$ and K_2HPO_4 react with each other, only one distinct compound should form. Hence, we conducted a conductimetric titration experiment by reacting $\text{Ga}(\text{NO}_3)_3$ and K_2HPO_4 in aqueous solution to determine the stoichiometric ratio of the Ga^{3+} cation to the HPO_4^{2-} anion in the $\text{Ga}_m(\text{HPO}_4)_n$. In principle, the electrical conductivity of a solution depends on the number of free ions and the charge of these ions. When a solid product is formed, the total number of free ions will fall accordingly to indicate the equivalent point of a stoichiometric ratio [23,24]. As shown in Figure 1, our conductimetric titration clearly showed a minimum conductivity point with a stoichiometric ratio of $\text{Ga}^{3+} : \text{HPO}_4^{2-}$ of 2:3, indicating the chemical composition of the reaction product to be $\text{Ga}_2(\text{HPO}_4)_3$. It is well-known that when $\text{Ga}(\text{NO}_3)_3$ and K_3PO_4 react with each other, the solid product formed has the chemical composition of

GaPO_4 . The difference between $\text{Ga}_2(\text{HPO}_4)_3$ and GaPO_4 —two solid-state Ga compounds of phosphates—is that $\text{Ga}_2(\text{HPO}_4)_3$ NPs can be readily prepared using the simple coprecipitation method in aqueous solution, whereas GaPO_4 NPs can only be synthesized using the hydrothermal method (vide infra).

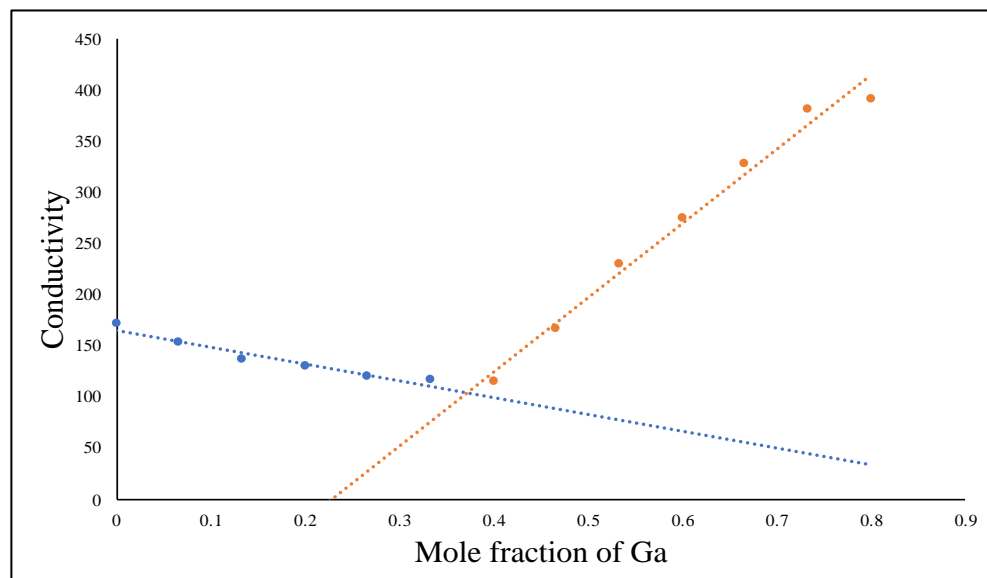


Figure 1. Curve of conductimetric titration measurements between $\text{Ga}(\text{NO}_3)_3$ and K_2HPO_4 , indicating the formation of the solid product $\text{Ga}_2(\text{HPO}_4)_3$. (the blue line represents the addition of Ga^{3+} ions, while the red line represents the addition of HPO_4^{2-} ions).

2.2. Synthesis of PVP-Coated $\text{Ga}_2(\text{HPO}_4)_3$ NPs Using the Coprecipitation Method

Through trial and error, we successfully synthesized stable $\text{Ga}_2(\text{HPO}_4)_3$ NPs using the coprecipitation method in the presence of polyvinylpyrrolidone (PVP) as a surface stabilizer. Specifically, $\text{Ga}_2(\text{HPO}_4)_3$ NPs were obtained by slowly adding an aqueous solution of $\text{Ga}(\text{NO}_3)_3$ (10 mM, 100 mL) containing 1 g of PVP (average MW = 8000) at the boiling point with another aqueous solution of K_2HPO_4 (30 mM, 100 mL) at the boiling point under vigorous stirring to afford a colorless colloidal solution with some turbidity. This solution immediately showed light scattering when a laser light was shone into it due to the Tyndall effect, indicating the formation of NPs in the solution (Figure S1). At this point, the pH of the resulting solution was about 6.9. After being stirred at 90 °C for 2 h and stored at room temperature overnight, the resultant NPs were dialyzed against distilled water using a cellulose tubular membrane to remove the byproducts and any unbound polymer. The solid product was collected after lyophilization. The Ga content of the powdered product was quantitatively analyzed using atomic absorption spectrometry (AAS). We noticed that the as-synthesized PVP-coated $\text{Ga}_2(\text{HPO}_4)_3$ NPs were stable in solution for over six months.

2.3. Characterization of PVP-Coated $\text{Ga}_2(\text{HPO}_4)_3$ NPs

The purified NPs were then characterized by Fourier transformed infrared spectroscopy (FT-IR), transmission electron microscopy (TEM) and energy-dispersive X-ray spectroscopy (EDS). First, the FT-IR spectrum of the PVP-coated $\text{Ga}_2(\text{HPO}_4)_3$ NPs contained the major characteristic vibrations of the PVP polymer, confirming the presence of PVP attached to the surfaces of $\text{Ga}_2(\text{HPO}_4)_3$ NPs (Figure 1). Note that the sample had been subjected to prolonged dialysis to remove the unbound PVP. In essence, the peak at 1645 cm^{-1} is attributable to the vibration of the carbonyl C=O group, while the peak at 2948 cm^{-1} is from the asymmetric stretching vibration of the CH_2 backbone of PVP, and the peak at 1288 cm^{-1} is due to the vibration of the amide group in the heterocyclic ring of PVP as shown in Figure 2 [25,26].

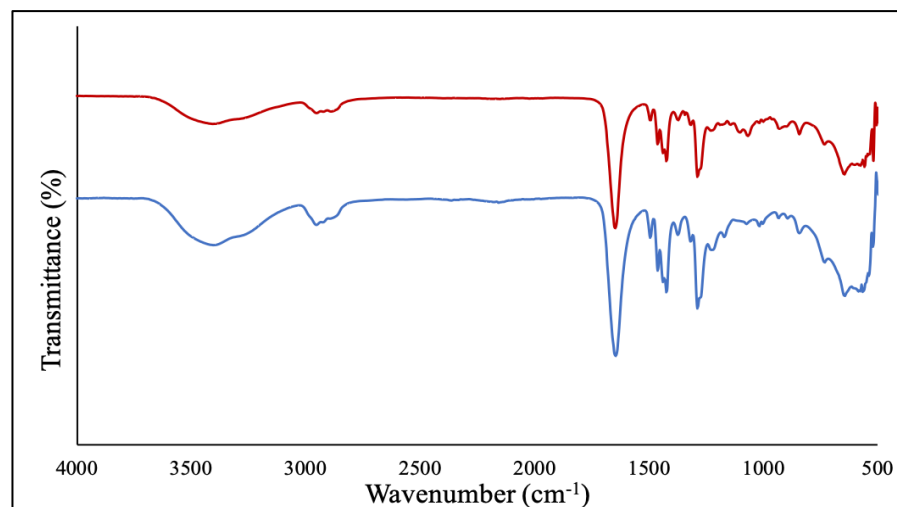


Figure 2. FT-IR spectrum of the PVP-coated $\text{Ga}_2(\text{HPO}_4)_3$ NPs (red) in comparison with that of the neat PVP (blue).

The size and morphology of PVP-coated $\text{Ga}_2(\text{HPO}_4)_3$ NPs were determined by TEM. The TEM images show that the NPs have an ill-defined semi-spherical shape, having a size ranging from 10 to 20 nm, with poor crystallinity (Figure 3). Additionally, the composition analysis by energy dispersive spectroscopy (EDS) from different selected areas of several NPs showed distinctive signals of elements Ga, P and O (Figure 3).

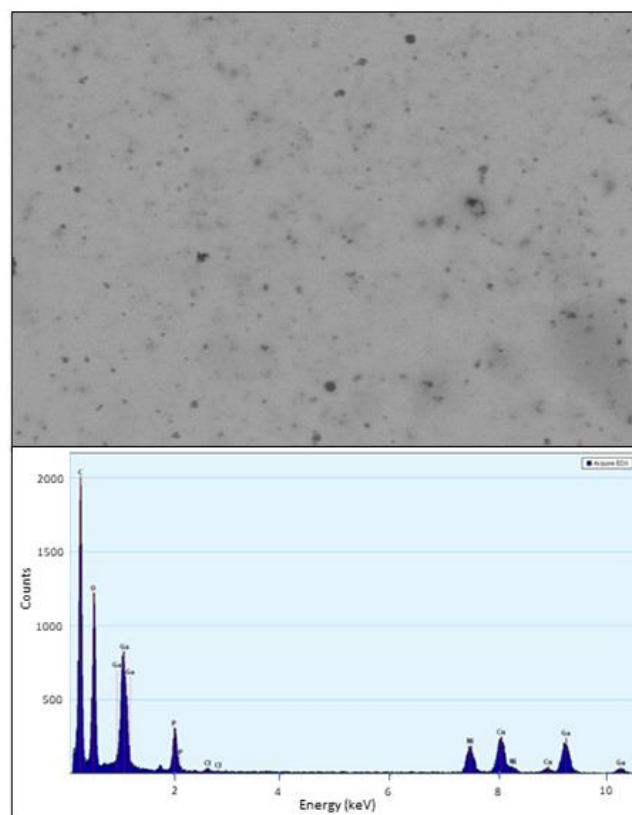


Figure 3. TEM images of PVP-coated $\text{Ga}_2(\text{HPO}_4)_3$ NPs (**top**) and a representative EDS spectrum of PVP-coated $\text{Ga}_2(\text{HPO}_4)_3$ NPs (**bottom**). Note: the signals of Cu and Ni are from the TEM grit.

2.4. Investigation of Antibacterial Activity of PVP-Coated $\text{Ga}_2(\text{HPO}_4)_3$ NPs

The minimum inhibitory concentration (MIC) of the PVP-coated $\text{Ga}_2(\text{HPO}_4)_3$ NPs against the Gram-negative *Pseudomonas aeruginosa* bacteria (ATCC 15692) was found to be $8 \mu\text{g}/\text{mL}$ (Figure 4). The optical density measurement obtained from the absorbance at 600 nm also confirmed the growth inhibition of *P. aeruginosa* by such NPs (Figure 4). A significant decrease in the optical densities was observed at around $8 \mu\text{g}/\text{mL}$ (i.e., $1 \times \text{MIC}$), and the higher concentrations, in sharp contrast to the control of untreated bacteria, suggest that PVP-coated $\text{Ga}_2(\text{HPO}_4)_3$ NPs may be a potent antimicrobial agent against *P. aeruginosa*. It should be noted that the MIC of $\text{Ga}(\text{NO}_3)_3$ measured by us under similar conditions using the same culture medium was found to be $12 \mu\text{g}/\text{mL}$, while this value decreased to $8 \mu\text{g}/\text{mL}$ when sodium citrate was added to the medium [27]. To further investigate the quantitative aspect of the antibacterial efficacy of the PVP-coated $\text{Ga}_2(\text{HPO}_4)_3$ NPs, both optical density values were measured, and colony-forming units (CFUs) were enumerated by plating $50 \mu\text{L}$ of each bacterial cultured treated with a specific concentration and incubation for 18 h. As shown in Figure 4, no bacterial colonies grew in the plates that had been inoculated with bacteria treated with the MIC value ($8 \mu\text{g}/\text{mL}$) or higher concentrations, confirming that the PVP-coated $\text{Ga}_2(\text{HPO}_4)_3$ NPs are indeed a potent antimicrobial agent against *P. aeruginosa*.

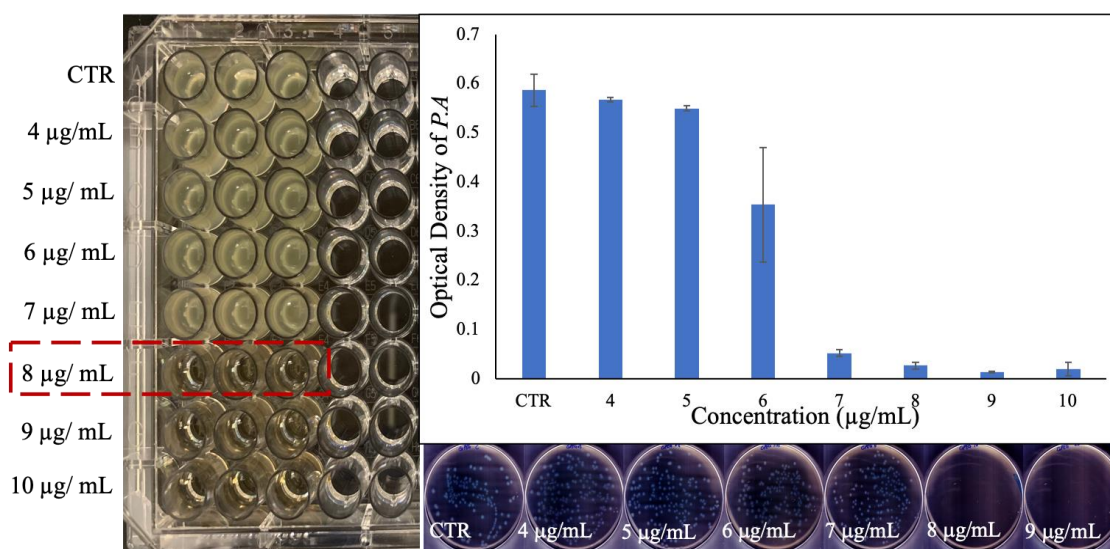


Figure 4. Results of the MIC determination for PVP-coated $\text{Ga}_2(\text{HPO}_4)_3$ NPs against *P. aeruginosa* using the broth dilution technique in the well-plate (left), the measured optical density values of the bacteria treated with various concentrations of NPs (top right), and the agar plates of the bacteria treated with different concentrations of NPs (down right).

To evaluate the kinetics of the Ga^{3+} release from such NPs, a volume of 10 mL of PVP-coated $\text{Ga}_2(\text{HPO}_4)_3$ NPs was sealed in a dialysis bag (MWCO = 12,000–14,000). The latter was submerged in 40 mL of citrate buffer solution with pH = 3.0 in a 55 mL test tube. The test tube was then placed in a shaker set at 37°C with a speed of 180 rpm. During the experiment, at predetermined intervals of 10, 20, 40, 60, 120, 240, 480, 960 and 1440 min, an aliquot of 2 mL solution was removed and treated with a drop of 70% concentrated nitric acid in preparation for gallium ion concentration analysis using atomic absorption spectrometry (AAS). All experiments were conducted in triplicate to ensure reproducibility and consistency in the results. As shown in Figure 5, the $\text{Ga}(\text{III})$ release underwent two different phases. First, within 4 h, the $\text{Ga}(\text{III})$ release rapidly reached the 60% level. Second, the remaining phase of $\text{Ga}(\text{III})$ release was considerably slower, i.e., it took 20 h for the $\text{Ga}(\text{III})$ release to reach from the 60% to the 100% level.

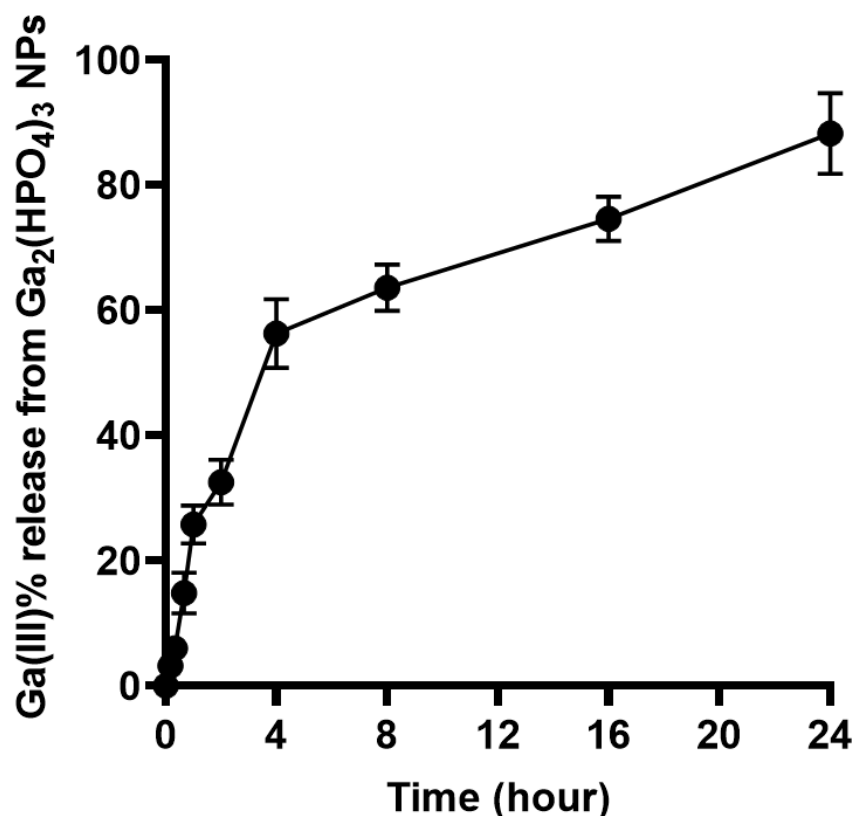


Figure 5. Percent Ga(III) release from PVP-coated Ga₂(HPO₄)₃ NPs versus time (hour).

Next, we investigated the antibacterial activity of PVP-coated Ga₂(HPO₄)₃ NPs against the Gram-positive *Staphylococcus aureus* bacteria (ATCC 6538) using the same experimental techniques as the above studies. However, our results showed no visible inhibition of bacterial growth at any of the concentrations we tested, including the highest possible concentration of 48 µg/mL (Figure S2). The measured optical density also showed no statistically significant decrease in the absorbance of 600 nm that was observed in this concentration range (Figure S2). Finally, the enumeration of CFUs obtained from the agar plates also failed to show any discernible inhibitory effect. Together, these results indicate that PVP-coated Ga₂(HPO₄)₃ NPs do not exhibit any significant antibacterial activity against the Gram-positive bacteria *S. aureus*, which becomes an obstacle to developing these NPs as a broad-spectrum antimicrobial agent.

It should be noted that the major difference between Gram-positive and Gram-negative bacteria is the thickness of the peptidoglycan layer and the existence or absence of an outer cell membrane in their cell wall. Compared to that of Gram-negative bacteria, the cell wall of Gram-positive bacteria has a thick multilayer of peptidoglycan outside the cell membrane [28]. We then speculated that the change of the surface-coating polymer from PVP to polyethylene glycol (PEG) might improve the ability of such NPs to penetrate the cell wall of Gram-positive bacteria. However, we were unable to prepare stable PEG-coated Ga₂(HPO₄)₃ NPs using the same coprecipitation method with PEG in place of PVP. We subsequently developed a top-down synthetic route to produce PEG-coated Ga₂(HPO₄)₃ NPs from the bulk samples using the sonication technique.

2.5. Synthesis of the Bulk Ga₂(HPO₄)₃ Sample

The bulk Ga₂(HPO₄)₃ sample was synthesized under the same conditions as described above for the synthesis of PVP-coated Ga₂(HPO₄)₃ NPs except that no surface-coating polymers were used. Specifically, the Ga₂(HPO₄)₃ precipitate was obtained by directly mixing an aqueous solution of Ga(NO₃)₃ (100 mM, 50 mL) at the boiling point with another aqueous solution of excess K₂HPO₄ (300 mM, 50 mL) at the boiling point. The mixing

resulted in the immediate formation of a white precipitate of $\text{Ga}_2(\text{HPO}_4)_3$. The product was filtered, washed thoroughly with deionized water to remove any unreacted salts and dried at $180\text{ }^\circ\text{C}$ for 4 h (Figure S3).

2.6. Synthesis of the PEG-Coated $\text{Ga}_2(\text{HPO}_4)_3$ NPs Using the Top-Down Sonication Method

The PEG-coated $\text{Ga}_2(\text{HPO}_4)_3$ NPs were produced by sonicating the bulk sample of K_2HPO_4 using DMSO the solvent and PEG (average MW = 8000) as the surface-coating agent, followed by sonication for 48 h to result in a translucent dispersion that also showed light scattering when a laser light was shone into it, confirming that size reduction of the particles occurred to produce NPs. The Ga content of these PEG-coated $\text{Ga}_2(\text{HPO}_4)_3$ NPs was determined using AAS.

2.7. Characterization of PEG-Coated $\text{Ga}_2(\text{HPO}_4)_3$ NPs

After purification by membrane dialysis, collection of the solid product was performed by lyophilization. Such NPs were first analyzed by FT-IR spectroscopy. As shown in Figure 6, the PEG-coated NPs contain all the major absorption bands of PEG, confirming that the polymer is bound to the surfaces of the NPs. Specifically, the characteristic absorption band at 2884 cm^{-1} is attributable to the vibration of stretching C–H. The observed bands at 1467 cm^{-1} and 1342 cm^{-1} are due to the C–H bending vibrations. The peaks at 1279 cm^{-1} and 1094 cm^{-1} are assigned to C–O–H [29].

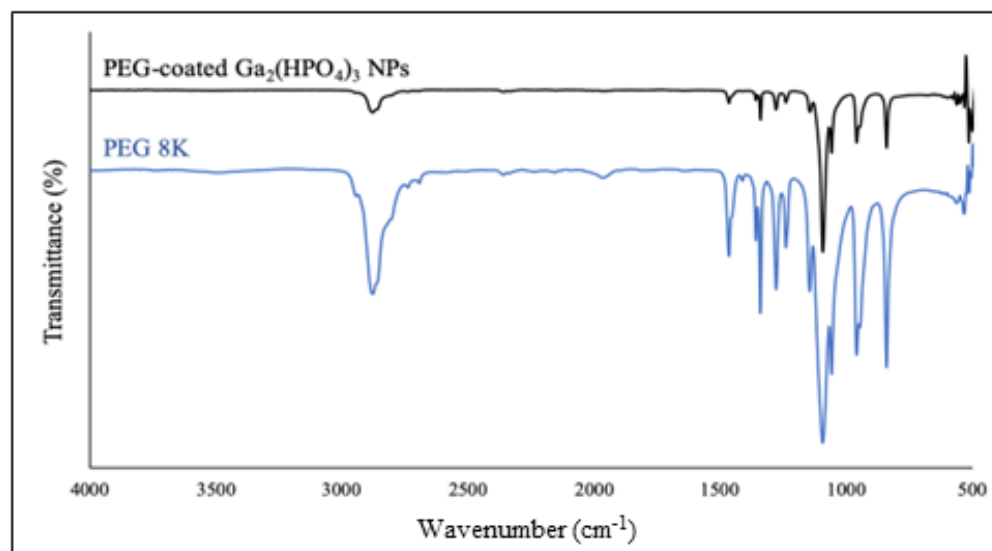


Figure 6. FT-IR spectrum of the PEG-coated $\text{Ga}_2(\text{HPO}_4)_3$ NPs (black) in comparison with that of the neat PVP (blue).

The TEM images show that the PEG-coated $\text{Ga}_2(\text{HPO}_4)_3$ NPs have quasi-spherical shapes with sizes $<10\text{ nm}$ (Figure 7a–e) and a relatively uniform shape and size distribution. At high magnification of the TEM, the images reveal a crystallinity of the $\text{Ga}_2(\text{HPO}_4)_3$ NPs. Moreover, the selected area electron diffraction (SAED) pattern consists of distinct diffraction points, indicating that such NPs are single crystallites (Figure 7f) [30]. On the other hand, the EDS measurements show distinctive signals of Ga, P and O, as shown in Figure 7.

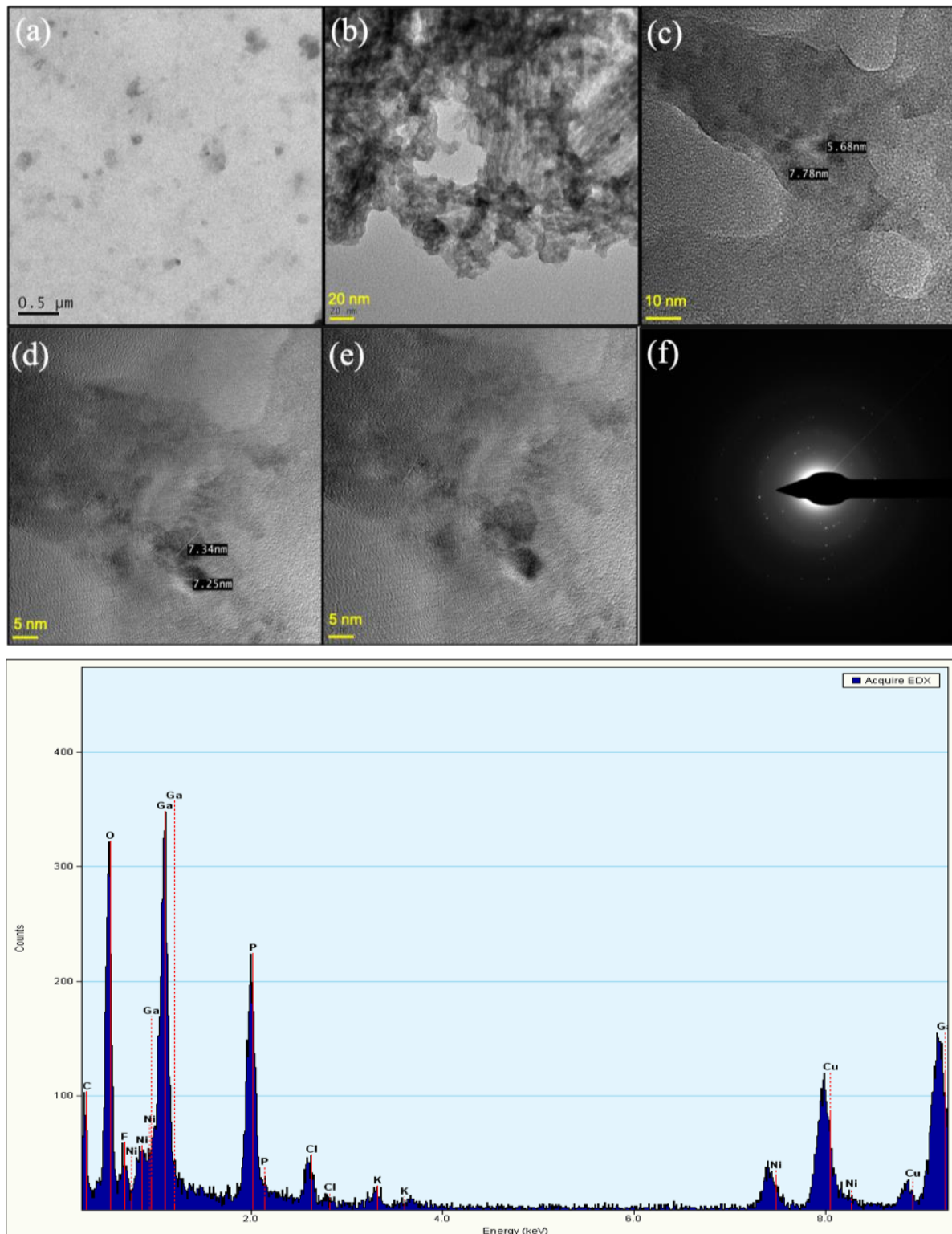


Figure 7. TEM images of PEG-coated $\text{Ga}_2(\text{HPO}_4)_3$ NPs with different magnifications (**top (a–e)**), the HRTEM image of single $\text{Ga}_2(\text{HPO}_4)_3$ NPs, showing the single crystal nature of such NPs (**top (f)**), and a representative EDS spectrum of PEG-coated $\text{Ga}_2(\text{HPO}_4)_3$ NPs (**bottom**). Note: the signals of Cu and Ni are from the TEM grit.

2.8. Investigation of Antibacterial Activity of PEG-coated $\text{Ga}_2(\text{HPO}_4)_3$ NPs

The MIC of the PEG-coated $\text{Ga}_2(\text{HPO}_4)_3$ NPs against the same strain of *P. aeruginosa* bacteria (i.e., ATCC 15692) that was used to determine the antimicrobial activity of the PVP-

coated $\text{Ga}_2(\text{HPO}_4)_3$ NPs in the above was found to be $8 \mu\text{g}/\text{mL}$ (Figure 8)—an identical value as that of PVP-coated $\text{Ga}_2(\text{HPO}_4)_3$, indicating that the change of surface-coating polymer from PVP to PEG does not have any discernible effect on the antimicrobial activity of $\text{Ga}_2(\text{HPO}_4)_3$ NPs against this Gram-negative strain of bacteria. This observation is also confirmed by measurements of both optical density values and CFUs (Figure 8).

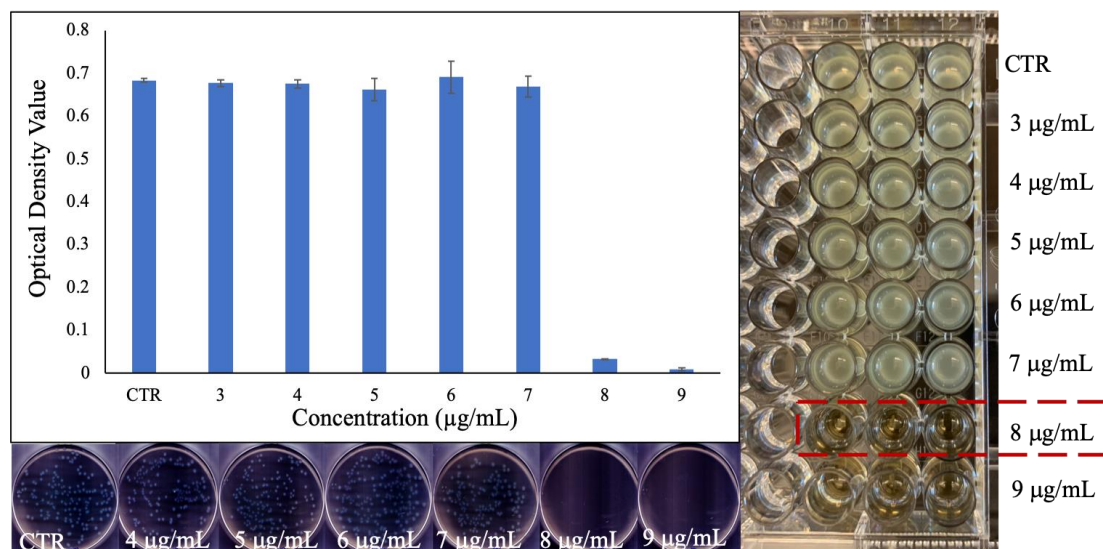


Figure 8. Results of the MIC determination for PEG-coated $\text{Ga}_2(\text{HPO}_4)_3$ NPs against *P. aeruginosa* using the broth dilution technique in the well-plate (right), the measured optical density values of the bacteria treated with various concentrations of NPs (top left), and the agar plates of the bacteria treated with different concentrations of NPs (down left).

Again, we investigated the antibacterial activity of PEG-coated $\text{Ga}_2(\text{HPO}_4)_3$ NPs against *S. aureus* bacteria (ATCC 6538) in the hope that the PEG surface coating would improve the interactions of these NPs with the thick multilayer of peptidoglycan interwoven with teichoic acid chains on the cell wall of Gram-positive bacteria. Unfortunately, all our experimental results, including the MIC determination, optical density measurements and CFU enumerations show that PEG-coated $\text{Ga}_2(\text{HPO}_4)_3$ NPs are not active against *S. aureus* bacteria (see Figure S4).

2.9. Investigation of Ga Resistance Development of PEG-Coated $\text{Ga}_2(\text{HPO}_4)_3$ NPs

The Ga resistance development of PEG-coated $\text{Ga}_2(\text{HPO}_4)_3$ NPs, in comparison with $\text{Ga}(\text{NO}_3)_3$ and ciprofloxacin, was examined in *P. aeruginosa* for a period of 30 days. The results show that the wild-type *P. aeruginosa* bacteria remain susceptible to PEG-coated $\text{Ga}_2(\text{HPO}_4)_3$ NPs after repetitive exposures to such NPs at the sub-lethal dose for 30 days, showing a remarkable reluctance to develop any Ga-resistant phenotypes. In sharp contrast, both $\text{Ga}(\text{NO}_3)_3$ and ciprofloxacin—one of the most frequently prescribed antibiotics in the clinical treatment of bacterial infections—exhibited a rapid development of drug resistance, attesting to the different antimicrobial mode of action by PEG-coated $\text{Ga}_2(\text{HPO}_4)_3$ vs. those of $\text{Ga}(\text{NO}_3)_3$ and ciprofloxacin (Figure 9).

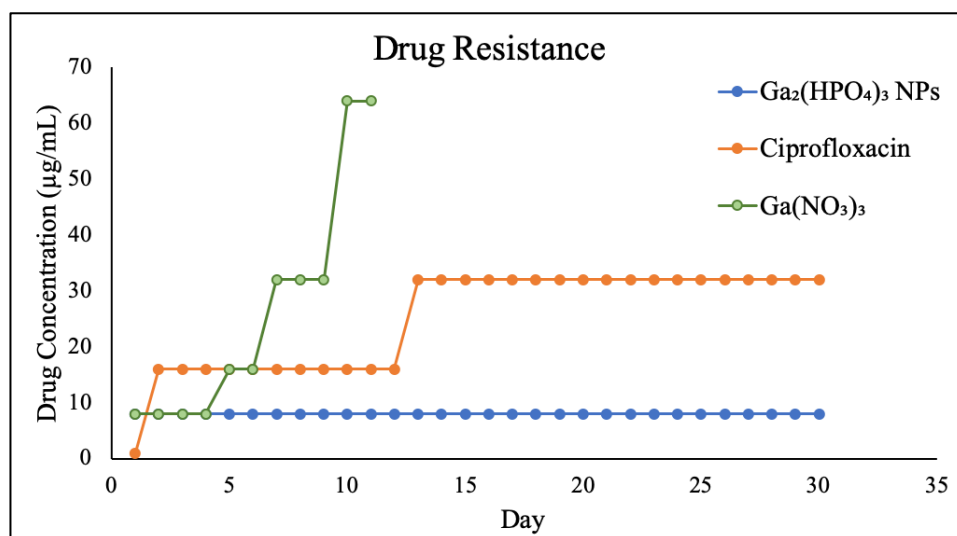


Figure 9. Results of Ga resistance development assays of PEG-coated Ga₂(HPO₄)₃ in comparison with Ga(NO₃)₃ and ciprofloxacin.

3. Conclusions

In conclusion, biocompatible Ga₂(HPO₄)₃ NPs that are surface functionalized with PVP or PEG can be readily prepared using either a direct coprecipitation method in aqueous solution or a top-down sonication technique. Both the PVP- and PEG-coated Ga₂(HPO₄)₃ NPs exhibit potent antimicrobial activity that is comparable to Ga(NO₃)₃ against *P. aeruginosa*. Similarly to Ga(NO₃)₃, these NPs remain ineffective against *S. aureus*. Nevertheless, our findings in this study strongly suggest that Ga-based NPs may represent a feasible solution to the various problems and shortcomings of molecular Ga compounds in the battle against AMR.

4. Materials and Methods

4.1. Chemical Reagents and Biological Materials

All chemical reagents were obtained from commercial sources and used without further purification. Gallium nitrate hydrate (Ga(NO₃)₃·xH₂O), dipotassium phosphate (K₂HPO₄), polyvinylpyrrolidone (PVP; average MW = 8000), polyethylene glycol (PEG; average MW = 8000), dimethyl sulfoxide (DMSO), gallium standard (1000 ± 10 µg/mL) were all purchased from Sigma-Aldrich. Bacterial strains, growth media and antibiotics, Gram-positive bacteria (ATCC 6538) and Gram-negative bacteria (ATCC 15692) were purchased from American Type Culture Collection. Tryptic broth powder (TSB), tryptic soy agar (TSA), nutrient broth (NB) and nutrient agar (NA) were purchased from Fisher Scientific.

4.2. Conductimetric Measurements to Determine the Stoichiometry

Solution conductivity measurements were employed to determine the stoichiometric ratio of a precipitate formed between Ga³⁺ and HPO₄²⁻. A solution of 1.0 mM K₂HPO₄ was titrated with a 1.0 mM solution of Ga(NO₃)₃ at 25 °C forming a white precipitate of Ga₂(HPO₄)₃ using an OAKTON PC 700 pH/Conductivity meter. The stoichiometric composition was determined by electrical conductivity in micro-siemens (µS) measured in 12 different titrations with different molar ratios of both reactants in each titration. The results of electrical conductivity readings were plotted against the mole ratio of Ga³⁺ ions to determine the stoichiometric ratio of Ga³⁺ and HPO₄²⁻.

4.3. Synthesis of PVP-Coated Ga₂(HPO₄)₃ NPs

A 100 mL aqueous solution containing 0.418 g of Ga(NO₃)₃ and 1 g of PVP (average MW = 8000) was heated to its boiling point and stirred at this temperature for 15 min.

Separately, a 100 mL aqueous solution of 1.3694 g of K_2HPO_4 was also heated to its boiling point. The gallium nitrate/polymer solution was added slowly into the dipotassium phosphate solution under vigorous stirring to give a colorless colloidal solution with some turbidity. After being heated on a hot plate at 90 °C for 2 h and stirred at room temperature overnight, the NP solution was dialyzed against distilled water using cellulose tubular membrane (MWCO = 12,000–14,000) to remove the byproducts and any unbound polymer. The PVP-coated $Ga_2(HPO_4)_3$ NPs were collected as a powdered product after lyophilization. The Ga content of the powdered product was quantitatively analyzed using atomic absorption spectrometry (AAS).

4.4. Synthesis of PEG-Coated $Ga_2(HPO_4)_3$ NPs

1 mg of the bulk $Ga_2(HPO_4)_3$ was added to 1 mL of DMSO in the presence of 100 mg of PEG (average MW = 8000) and sonicated for 48 h. The resulting suspension was clear and showed light scattering when a laser light was shone to it, indicating the formation of NPs. The PEG-coated $Ga_2(HPO_4)_3$ NPs were collected as a powdered product after lyophilization. The Ga content of the powdered product was quantitatively analyzed using atomic absorption spectrometry (AAS).

4.5. TEM and HRTEM Imaging Studies

The NPs were first dispersed in ethanol (95%) and sonicated for 30 min. Next, one drop of NP suspension was placed onto a carbon-coated copper TEM grid (400 mesh) and allowed to air-dry before the analysis. The TEM specimens were imaged using an FEI Tecnai F20 Transmission Electron Microscope equipped with a field emission gun and analyzed at 200 KV. The energy dispersive X-ray spectroscopic (EDX) data were acquired for a selected area of the sample with the integrated scanning TEM (STEM) unit and attached EDAX spectrometer. The spatial resolution is <1 nm through the acquisition of high resolution with high-angle angular dark field (HAADF) images, which are sensitive to atomic number (Z) contrast.

4.6. Antibacterial Activity Assays

The bacteria were cultured in tryptic soy broth (TSB) for Bacterial *S. aureus* SA (ATCC 6538) and nutrient broth (NB) for *P. aeruginosa* (ATCC 15692), respectively. The bacterial suspension was prepared by transferring an isolated colony from a streak plate of tested bacterial strain into 5 mL of TSB media, followed by incubation at 37 °C with shaking at 180 rpm for 18 h. Next, 50 µL was sub-cultured in 5 mL fresh TSB media and incubated for additional 4 h. The cell density of bacterial suspension after incubation was 10^9 CFU/mL. Tested bacterial cell concentrations for studies were adjusted to have a final concentration of bacteria in the tested suspension to be at 10^6 CFU/mL.

4.7. MIC Assays

The bacterial suspension cultured overnight was adjusted to the targeted bacterial concentration of 10^6 CFU/mL. Next, drugs to be tested were added to the bacterial suspension, and the final concentration of DMSO in the bacterial suspension is 0.2% in 96-well plates. Following the treatment with drugs, bacteria were incubated for 18 h at 37 °C and shaking speed 180 rpm. The MIC was determined as the lowest concentration that shows no visible bacterial growth with unaided eyes.

4.8. Colony Forming Unit (CFU/mL) Assays

Bacteria grown in the cell culture medium without NPs were used as the control in all such experiments. After 18 h of incubation, a diluted mixture containing the appropriate amount of NPs was spread across the agar plate using a glass spreader. The colonies found in each plate were then counted and converted to numbers of CFU/mL. Triplicates were obtained for all technical and biological parameters.

4.9. Drug Resistance Development Assays

Typically, in 96-well plates, serial twofold dilutions of tested drugs with a bacterial strain were prepared to have the targeted bacterial cell concentration of 10^6 CFU/mL. The bacterial suspensions were added in triplicate to 96-well plates and incubated overnight in an incubator at 37 °C with shaking speed at 180 rpm. A bacterial suspension without drug was used as a negative control. After 18 h of incubation, the MIC was determined by measuring the O.D. value using a microplate reader in which the lowest concentration of the drug that has an O.D. reading similar to the control is the MIC. Next, 10 μ L of the sub-MIC was incubated with the tested drug and incubated to determine the MIC. This procedure was repeated for 30 days to test the potential ability of tested bacteria to develop resistance to the drug. A SpectraMax M4 Spectrophotometer was used to measure absorbance in the 96-well plates.

Supplementary Materials: The following supporting information can be downloaded at: <https://www.mdpi.com/article/10.3390/antibiotics12111578/s1>, All data generated or analyzed during this study are included in this published article and its supplementary information files are available free of charge. Figure S1: Schematic of the synthesis of PVP-coated Ga₂(HPO₄)₃ NPs with the Tyndall effect exhibited by the product. Figure S2: Results of the MIC determination for PVP-coated Ga₂(HPO₄)₃ NPs against *S. aureus* using the broth dilution technique in the well-plate (left) and the measured optical density values of the bacteria treated with various concentrations of NPs. Figure S3: Schematic of the two-step synthesis of PEG-coated Ga₂(HPO₄)₃ NPs with the Tyndall effect exhibited by the product: (A) the preparation of the bulk sample and (B) the synthesis of PEG-coated Ga₂(HPO₄)₃ NPs. Figure S4: Results of the MIC determination for PEG-coated Ga₂(HPO₄)₃ NPs against *S. aureus* using the broth dilution technique in the well-plate (left) and the measured optical density values of the bacteria treated with various concentrations of NPs.

Author Contributions: S.D.H. was primarily responsible for the conception of the project; H.A. contributed to the design of all experiments, including the synthesis and characterization of the nanomaterials; G.C. performed the experiments to confirm the in vitro antimicrobial activity of the nanomaterials; S.D.H. and H.A. produced the manuscript with contributions and feedback of all authors. All authors have read and agreed to the published version of the manuscript.

Funding: This research receives no external funding.

Institutional Review Board Statement: Not applicable.

Informed Consent Statement: Not applicable.

Data Availability Statement: All data generated or analyzed during this study are included in this published article and its Supplementary Information Files.

Acknowledgments: The Cryo TEM Facility at KSU's Advanced Materials and Liquid Crystal Institute (AMLCI), which is supported by the Ohio Research Scholars Program, was used to obtain the TEM results reported in this paper.

Conflicts of Interest: The authors declare no conflict of interest.

References

1. Norrby, S.R.; Nord, C.E.; Finch, R. Lack of development of new antimicrobial drugs: A potential serious threat to public health. *Lancet Infect. Dis.* **2005**, *5*, 115–119. [[CrossRef](#)] [[PubMed](#)]
2. Flamm, R.K.; Weaver, M.K.; Thornsberry, C.; Jones, M.E.; Karlowsky, J.A.; Sahm, D.F. Factors associated with relative rates of antibiotic resistance in *Pseudomonas aeruginosa* isolates tested in clinical laboratories in the United States from 1999 to 2002. *Antimicrob. Agents Chemother.* **2004**, *48*, 2431–2436. [[CrossRef](#)] [[PubMed](#)]
3. DeLeon, K.; Balldin, F.; Watters, C.; Hamood, A.; Griswold, J.; Sreedharan, S.; Rumbaugh, K.P. Gallium maltolate treatment eradicates *Pseudomonas aeruginosa* infection in thermally injured mice. *Antimicrob. Agents Chemother.* **2009**, *53*, 1331–1337. [[CrossRef](#)]
4. Aslam, B.; Wang, W.; Arshad, M.I.; Khurshid, M.; Muzammil, S.; Rasool, M.H.; Nisar, M.A.; Alvi, R.F.; Aslam, M.A.; Qamar, M.U.; et al. Antibiotic resistance: A rundown of a global crisis. *Infect. Drug Resist.* **2018**, *11*, 1645–1658. [[CrossRef](#)]
5. Lewis, K. Platforms for Antibiotic Discovery. *Nat. Rev. Drug Discov.* **2013**, *12*, 371–387. [[PubMed](#)]

6. Frei, A.; Zuegg, J.; Elliott, A.G.; Baker, M.; Braese, S.; Brown, C.; Chen, F.; Dowson, G.C.; Dujardin, G.; Jung, N.; et al. Metal Complexes as a Promising Source for New Antibiotics. *Chem. Sci.* **2020**, *11*, 2627–2639. [[CrossRef](#)]
7. Frei, A.; Verderosa, A.D.; Elliott, A.G.; Zuegg, J.; Blaskovich, M.A.T. Metals to Combat Antimicrobial Resistance. *Nat. Rev. Chem.* **2023**, *7*, 202–224.
8. Kaneko, Y.; Thoendel, M.; Olakanmi, O.; Britigan, B.E.; Singh, P.K. The transition metal gallium disrupts *Pseudomonas aeruginosa* iron metabolism and has antimicrobial and antibiofilm activity. *J. Clin. Investig.* **2007**, *117*, 877–888. [[CrossRef](#)]
9. Kelson, A.B.; Carnevali, M.; Truong-Le, V. Gallium-based anti-infectives: Targeting microbial iron-uptake mechanisms. *Curr. Opin. Pharmacol.* **2013**, *13*, 707–716. [[CrossRef](#)]
10. Richter, K.; Thomas, N.; Claeys, J.; McGuane, J.; Prestidge, C.A.; Coenye, T.; Wormald, P.-J.; Vreugde, S. A Topical Hydrogel with Deferiprone and Gallium-Protoporphyrin Targets Bacterial Iron Metabolism and Has Antibiofilm Activity. *Antimicrob. Agents Chemother.* **2017**, *61*, e00481-17.
11. Goss, C.H.; Kaneko, Y.; Khuu, L.; Anderson, G.D.; Ravishankar, S.; Aitken, M.L.; Lechtzin, N.; Zhou, G.; Czyn, D.M.; McLean, K.; et al. Gallium disrupts bacterial iron metabolism and has therapeutic effects in mice and humans with lung infections. *Sci. Transl. Med.* **2018**, *10*, eaat7520. [[CrossRef](#)]
12. Ratledge, C.; Dover, L.G. Iron metabolism in pathogenic bacteria. *Annu. Rev. Microbiol.* **2000**, *54*, 881–941.
13. Weaver, K.D.; Heymann, J.J.; Mehta, A.; Roulhac, P.L.; Anderson, D.S.; Nowalk, A.J.; Adhikari, P.; Mietzner, T.A.; Fitzgerald, M.C.; Crumbliss, A.L. Ga³⁺ as a mechanistic probe in Fe³⁺ transport: Characterization of Ga³⁺ interaction with FbpA. *J. Biol. Inorg. Chem.* **2008**, *13*, 887–898. [[CrossRef](#)]
14. Chitambar, C.R. Gallium and its competing roles with iron in biological systems. *Biochim. Biophys. Acta* **2016**, *1863*, 2044–2053. [[CrossRef](#)]
15. Bernstein, L.R. Mechanisms of Therapeutic Activity for Gallium. *Pharmacol. Rev.* **1998**, *50*, 665–682. [[PubMed](#)]
16. Minandri, F.; Bonchi, C.; Frangipani, E.; Imperi, F.; Visca, P. Promises and failures of gallium as an antibacterial agent. *Future Microbiol.* **2014**, *9*, 379–397. [[CrossRef](#)] [[PubMed](#)]
17. Bernstein, L.R.; Tanner, T.; Godfrey, C.; Noll, B. Chemistry and Pharmacokinetics Of Gallium Maltolate, A Compound With High Oral Gallium Bioavailability. *Met.-Based Drugs* **2000**, *7*, 33–47. [[CrossRef](#)] [[PubMed](#)]
18. Banin, E.; Lozinski, A.; Brady, K.M.; Berenshtein, E.; Butterfield, P.W.; Moshe, M.; Chevion, M.; Greenberg, E.P.; Banin, E. The potential of desferrioxamine-gallium as an anti-*Pseudomonas* therapeutic agent. *Proc. Natl. Acad. Sci. USA* **2008**, *105*, 16761–16766. [[CrossRef](#)]
19. Lessa, J.A.; Parrilha, G.L.; Beraldo, H. Gallium complexes as new promising metallodrug candidates. *Inorg. Chim. Acta* **2012**, *393*, 53–63. [[CrossRef](#)]
20. Miller, K.P.; Wang, L.; Benicewicz, B.C.; Decho, A.W. Inorganic nanoparticles engineered to attack bacteria. *Chem. Soc. Rev.* **2015**, *44*, 7787–7807.
21. Gao, W.; Thamphiwatana, S.; Angsantikul, P.; Zhang, L. Nanoparticle approaches against bacterial infections. *Wiley Interdiscip. Rev. Nanomed. Nanobiotechnol.* **2014**, *6*, 532–547. [[CrossRef](#)] [[PubMed](#)]
22. Wang, Z.; Yu, B.; Alamri, H.; Yarabarla, S.; Kim, M.H.; Huang, S.D. KCa(H₂O)₂[Fe(III)(CN)₆]H₂O Nanoparticles as an Antimicrobial Agent against *Staphylococcus aureus*. *Angew. Chem. Int. Ed. Engl.* **2018**, *57*, 2214–2218. [[CrossRef](#)] [[PubMed](#)]
23. Kolthoff, I.M. Conductometric Titrations. *Ind. Eng. Chem.* **1930**, *2*, 225–230. [[CrossRef](#)]
24. McCurdy, W.H.; Galt, J. Improved Conductometric Titration of Weak Bases. *Anal. Chem.* **1958**, *30*, 940–946. [[CrossRef](#)]
25. Song, Y.-J.; Wang, M.; Zhang, X.-Y.; Wu, J.-Y.; Zhang, T. Investigation on the role of the molecular weight of polyvinyl pyrrolidone in the shape control of high-yield silver nanospheres and nanowires. *Nanoscale Res. Lett.* **2014**, *9*, 17. [[CrossRef](#)]
26. Koczur, K.M.; Mourdikoudis, S.; Polavarapu, L.; Skrabalak, S.E. Polyvinylpyrrolidone (PVP) in nanoparticle synthesis. *Dalton Trans.* **2015**, *44*, 17883–17905. [[CrossRef](#)]
27. Wang, Z.; Li, J.; Benin, B.M.; Yu, B.; Bunge, S.D.; Abeydeera, N.; Huang, S.D.; Kim, M.H. Lipophilic Ga Complex with Broad-Spectrum Antimicrobial Activity and the Ability to Overcome Gallium Resistance in both *Pseudomonas aeruginosa* and *Staphylococcus aureus*. *J. Med. Chem.* **2021**, *64*, 9381–9388. [[CrossRef](#)]
28. Pajerski, W.; Ochonska, D.; Brzychczy-Wloch, M.; Indyka, P.; Jarosz, M.; Golda-Cepa, M.; Sojka, Z.; Kotarba, A. Attachment efficiency of gold nanoparticles by Gram-positive and Gram-negative bacterial strains governed by surface charges. *J. Nanoparticle Res.* **2019**, *21*, 186. [[CrossRef](#)]
29. Shameli, K.; Ahmad, M.B.; Jazayeri, S.D.; Sedaghat, S.; Shabanzadeh, P.; Jahangirian, H.; Mahdavi, M.; Abdollahi, Y. Synthesis and characterization of polyethylene glycol mediated silver nanoparticles by the green method. *Int. J. Mol. Sci.* **2012**, *13*, 6639–6650. [[CrossRef](#)]
30. Kurtjak, M.; Vukomanovic, M.; Kramer, L.; Suvorov, D. Biocompatible nano-gallium/hydroxyapatite nanocomposite with antimicrobial activity. *J. Mater. Sci. Mater. Med.* **2016**, *27*, 170. [[CrossRef](#)]

Disclaimer/Publisher's Note: The statements, opinions and data contained in all publications are solely those of the individual author(s) and contributor(s) and not of MDPI and/or the editor(s). MDPI and/or the editor(s) disclaim responsibility for any injury to people or property resulting from any ideas, methods, instructions or products referred to in the content.